Article

The International Journal of Robotics Research
2014, Vol. 33(6) 847–865

DOI: 10.1177/0278364913517952
ijr.sagepub.com

Absolutely stable model-based 2-port force controller for telerobotic applications

J. Scot Hart[1] and Günter Niemeyer[2]

Abstract

Large industrial-like slave robots pose a challenging problem for telerobotic control designers focused on achieving good transparency. The human operator typically feels both the large friction forces and heavy inertial forces inherent to these robots. Force control can be used to attempt and hide these internal forces from the user, but force control is a challenging design problem, especially in situations like telerobotics where it is not clear what the environmental impedance will be at any given moment.

This paper introduces a model-based force controller designed to reject the friction in slave robots to improve the overall transparency of the telerobotic system. The primary objective of the force controller is to ensure the closed loop slave 2-port is absolutely stable such that the controller maintains the robustness of the overall telerobot. An analysis is provided that shows that, in order to achieve absolute stability, a local slave-side force controller cannot hide any of the robot's inertial forces. It is from this result that model-based force control gets its name as it uses a model of the robot's inertial properties to reject friction forces without attempting to reject inertial forces.

Keywords

Telerobotics, force control, dexterous manipulation, model based control, 2-port, absolute stability

1. Introduction

Ideally telerobotic systems would provide exact position and force tracking from the human user to the remote environment in order to feel completely transparent. While much work has focused on producing control systems designed to optimize the transparency of telerobots, it is clear that when dealing with real systems subject to unmodeled dynamics and unavoidable phase lags that there is a fundamental trade off between transparency and robustness.

While there are many different types of telerobotic controllers, one constant among all these controllers is that the more transparent the master and slave robots are to start with (i.e. the lower the mass and friction, and the higher the stiffness) the more transparent the telerobotic system can be made given a desired robustness. Many telerobots however are designed to do heavy work in harsh environments (Akin, 2001). These telerobots, such as the one pictured in Figure 1, typically use slave devices with heavy and stiff linkages paired with highly geared actuators resulting in both large inertial and friction forces.

In order to increase the transparency of such telerobots without reducing robustness, this paper presents a local force control loop for the slave robot that increases the transparency of the slave while ensuring the 2-port system representing the combination of force controller and slave is absolutely stable. To maintain absolute stability, the force controller uses a model of the inertial properties of the robot to focus on rejecting the friction and unwanted damping in the system without attempting to reject inertial forces. Since the resulting system is absolutely stable, it can be easily added to passivity based telerobotic controllers (Anderson and Spong, 1989; Niemeyer and Slotine, 2004; Ryu et al., 2004; Tanner and Niemeyer, 2004; Franken et al., 2011), and can even produce transparency increases with little to no loss of robustness in controllers where passivity is not the primary design objective.

1.1. Background: Robotic force control

Despite the name, robotic force control is typically not a question of getting a robot to apply a desired force, but more of a question of how to get the robot to move in and interact with an unknown environment in a useful way. As such,

[1]Optimedica Corp., Sunnyvale, CA, USA
[2]Disney Research, Glendale, CA, USA

Corresponding author:
J. Scot Hart, Optimedica Corp., 1310 Moffett Park, Sunnyvale, CA 94089, USA.
Email: hartj@alumni.stanford.edu

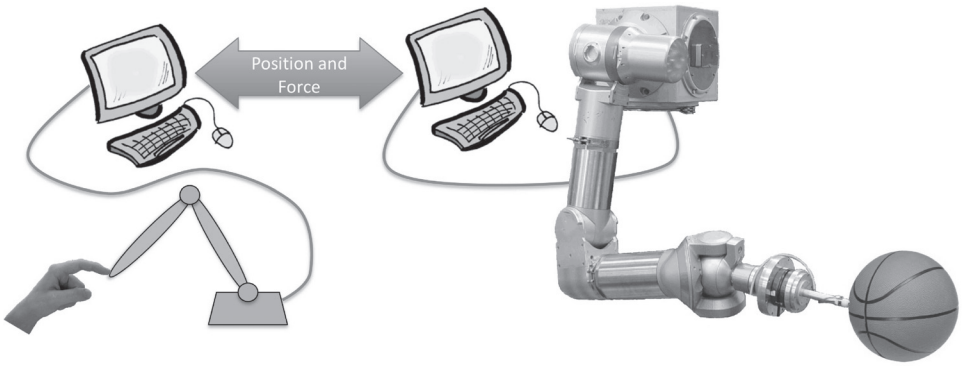

Fig. 1. A bilateral telerobotic system using Ranger as the slave device. Ranger was designed and built by the University of Maryland's Space Systems lab for servicing of satellites in orbit.

the majority of robotic force control work can be loosely categorized into two approaches. The first approach uses the force sensor to give position-controlled robots the ability to accommodate unexpected contact forces. Examples include stiffness (Salisbury, 1980) and impedance control (Hogan, 1985a,b,c), both of which act to shape the closed loop impedance of the robot.

The second approach focuses on explicit force tracking when the robot is known to be in contact with its environment. Since it is rarely desirable to control forces in every direction at once, hybrid control (Raibert and Craig, 1981; Khatib, 1987) breaks up the manipulation task into force-controlled and position-controlled directions.

While several studies have shown stability of stiffness, impedance, and hybrid controllers for robots modeled with rigid links (Hogan, 1988; Kazerooni et al., 1990; Wen and Murphy, 1991), these studies often do not predict the contact instabilities seen when force-controlled robots interact with stiff environments. To explain contact instability, the model of the robot must be expanded to include unmodeled phase lags and structural compliance in the robot (Eppinger and Seering, 1992). Furthermore, Colgate and Hogan have shown that when these higher order dynamics are accounted for there is a limit to how much of the inertial forces a force controller can hide while guaranteeing stability when interacting with all possible environments (Colgate and Hogan, 1989).

Based on Colgate and Hogan's results, Newman introduced natural admittance control (NAC) (1992; 1994) as a means of guaranteeing stability for all environments. By ensuring the closed-loop robot always has the same or greater effective mass than the open-loop robot, the system is provably passive and therefore stable in contact with all passive environments.

Alternate force control approaches make the trade-off between performance and robustness by estimating the properties of the environment on the fly and adjusting the control algorithms appropriately. Examples include switching controllers (Mills and Lokhorst, 1993), and adaptive controllers (Singh and Popa, 1995; Roy and Whitcomb, 2002).

1.1.1. Force sensing in telerobotics Telerobots differ from autonomous robots in that the cognitive abilities required to interact with an unstructured environment are typically provided by the human operator and not by the control system. As such the use of force sensing in telerobotics is typically focused on improving system transparency as opposed to shaping system dynamics.

The 4- and 3-channel controllers that theoretically provide perfect transparency require force measurements (Lawrence, 1993; Yokokohji and Yoshikawa, 1994; Hashtrudi-Zaad and Salcudean, 2002), yet as with autonomous robots the addition of force feedback often results in contact instability when contacting stiff environments (Daniel and McAree, 1998).

Several approaches have been taken to achieve the transparency gains made possible by force feedback without reducing robustness. Adaptive telerobotic controllers (Love and Book, 2004; Park and Khatib, 2006; Richert et al., 2012) estimate environment stiffness and adjust control gains on the fly, while additional modeling can help predict and subtract unwanted motions (Kuchenbecker and Niemeyer, 2006).

Perhaps the most robust way to improve transparency however is to bypass force feedback and instead focus on modeling and rejecting the friction in the system (Mahvash and Okamura, 2006, 2007). Unfortunately these friction models are unique to each robot and can be quite complex and difficult to develop (Olsson et al., 1998).

1.2. Local slave-side force control

Figure 2 presents a n-DOF force-controlled slave device and its connections to the outside world. The m-dimensional (where $m \leq n$) vectors x_a and $\dot{x}_a$ represent the Cartesian space position and velocity of the end-effector based on measurements of the joint positions q at the actuators. In this paper, the subscript a stands for actuator and indicates a position or force that is either applied by or measured at the actuators. The Cartesian space position and velocity of the end-effector relative to the environment are given by x_e and $\dot{x}_e$ where the subscript e stands for environment and is

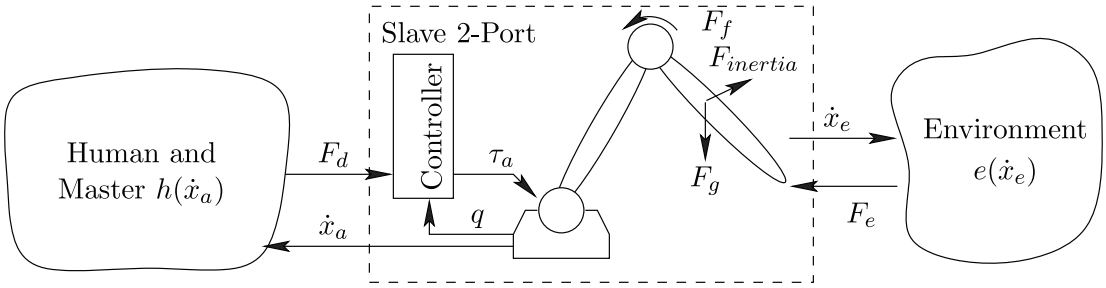

Fig. 2. Slave device dynamically interacting with both the environment as well as the rest of the teleoperator.

used to indicate a force or position at the interface between the robot and the environment.

We find x_a using the forward kinematics of the robot.

$$x_a = f_{fk}(q) \tag{1}$$

Since the model used to derive the forward kinematics usually makes several assumptions, such as rigid links and backlash-less actuators, x_a is typically only an estimate of x_e. Similarly $\dot{x}_a$ is found using the robot's Jacobian matrix $J(q)$ and is typically only an estimate of $\dot{x}_e$.

$$\dot{x}_a = J(q)\,\dot{q} \tag{2}$$

Since the large industrial-like robots considered here are quite stiff, it is safe to assume the difference between x_a and x_e is small and that the robot provides almost perfect position tracking. To improve transparency therefore, the force controller should focus on force tracking by providing a set of actuator torques τ_a that makes the environment force F_e track the desired force F_d as close as possible.

In addition to the environmental and actuator torques, the slave is also subject to frictional forces F_f, gravitational forces F_g, and inertial forces $F_{inertia}$. Assuming the gravitational forces are well known and compensated for, the objective of force tracking can be reduced to rejecting friction forces and hiding inertial forces based on sensor measurements of F_e and q.

To analyze the system, we view the closed-loop slave as a 2-port device, a modeling technique borrowed from electrical network theory and first used to model telerobotic systems by Hannaford (1989). In this case we will model the slave robot as a 2-port admittance device

$$\begin{aligned} \dot{x}_a &= y_{11}(F_d) - y_{12}(F_e) \\ \dot{x}_e &= y_{21}(F_d) - y_{22}(F_e) \end{aligned} \tag{3}$$

which exchanges power with two independent 1-port impedances that represent the rest of the teleoperator, including the master device which is held by the user, and the environment.

$$F_d = h(\dot{x}_a) \quad F_e = e(\dot{x}_e) \tag{4}$$

Here the functions $y_{ij}(F)$ represent the closed-loop admittance parameters of the slave 2-port while $h(\dot{x})$ and $e(\dot{x})$ are the impedances of the human operator, as seen through the rest of the teleoperator, and the environment respectively. Note the admittances $y_{11}(F)$ and $y_{22}(F)$ relate velocities to locally applied forces, while $y_{12}(F)$ and $y_{21}(F)$ relate the velocity at one side of the robot to a force applied at the other side.

As admittance is a measurement of ease of motion, the larger the 2-port admittance functions, the more transparent the robot. Both friction and inertial forces reduce the transparency of a slave robot and as such, their effect on the system can be seen as a reduction in the admittances $y_{ij}(F)$. The objective of increasing transparency can therefore be re-stated as a desire for increasing the closed-loop admittance functions $y_{ij}(F)$ as much as possible.

Of course the admittance functions cannot be increased without limit as stability issues will always arise. In particular, the difficulty in designing force control algorithms for slave robots is that, due to the unconstrained nature of teleoperation, there is no prior knowledge as to what the environment and human impedances will be at any given moment. Without this knowledge it is necessary to ensure the closed-loop slave system will be stable for all possible combinations of $e(\dot{x}_e)$ and $h(\dot{x}_a)$.

1.3. Passivity and absolute stability

Proving stability for all possible combinations of $e(\dot{x}_e)$ and $h(\dot{x}_a)$ can be quite complicated. Furthermore true stability, as defined by convergence to a particular equilibrium state, is both undesirable and impossible to ensure when accounting for unknown human inputs.

More realistically, we wish to prove that the telerobot's motions and contact forces are predictable and easily controlled by the human operator at all times regardless of the environment's impedance. One method to obtain this desired controllability is to require the telerobot to be passive such that it cannot generate any energy which could drive the system unstable.

If the stored energy at time $t = 0$ can be assumed to be zero, this is equivalent to requiring that the net energy flow into the system is always greater then zero.

$$\int_0^t \left(F_d^{\mathrm{T}}\dot{x}_a - F_e^{\mathrm{T}}\dot{x}_e\right) d\tau \geq 0 \tag{5}$$

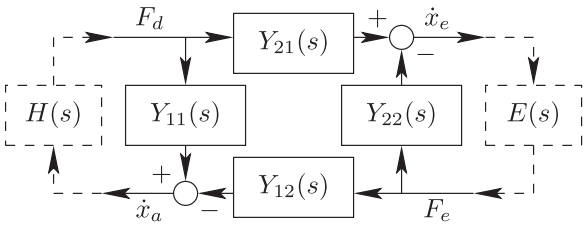

Fig. 3. 2-port admittance parameter transfer functions.

For the cases where the telerobot can be modeled as linear time-invariant (LTI) system the admittance functions $y_{ij}(F)$ can be expressed as transfer functions $Y_{ij}(s)$. Similarly, if the environment and human impedances can be modeled as LTI, the impedances $e(\dot{x})$ and $h(\dot{x})$ become the transfer functions $E(s)$ and $H(s)$ respectively. The resulting LTI system representing the closed-loop slave 2-port can now be expressed using the block diagram of Figure 3.

For such an LTI system, passivity can be shown by checking for positive realness. For example, an LTI 1-port, such as the environment, is passive if its transfer function $E(s)$ is positive real.

$$\Re(E(s)) \geq 0 \quad \text{if} \quad \Re(s) \geq 0 \tag{6}$$

From a frequency domain perspective positive realness can be expressed as a limitation on the phase of the frequency response.

$$-90^\circ \leq \angle E(i\omega) \leq 90^\circ \tag{7}$$

Similarly for the slave robot to be passive its 2-port admittance matrix given by

$$Y(s) = \begin{bmatrix} Y_{11}(s) & Y_{12}(s) \\ Y_{21}(s) & Y_{22}(s) \end{bmatrix} \tag{8}$$

must be a positive real matrix (Slotine and Li, 1991). To be positive real the poles of all elements in the matrix $Y(s)$ must be in the left half plane and $Y(s)+Y(s^*)$ must be positive semi-definite for $Re(s) > 0$, where s^* is the complex conjugate of the Laplace operator s.

While passivity guarantees a well-behaved teleoperator it also provides some potentially unwanted limitations. In particular a passive telerobot does not allow for power scaling. If a passive telerobot scales up the user's motions at the remote site then it must also scale down the output forces such that the power output at the remote site does not exceed the power input from the user. This is in contrast to the more typically desired situation where both position and force are scaled in the same direction.

A more practical requirement to ensure the telerobot will be well behaved is to require that all passive environments the telerobot interacts with are mapped to a passive admittance as seen by the human operator. A 2-port system that maintains this passive mapping is said to be absolutely stable (Llewellyn, 1952). Absolute stability allows the 2-port to generate energy as long as it is not readily apparent to the outside world that energy is being generated. Furthermore absolute stability also ensures any passive human impedance $h(\dot{x}_a)$ will map to a passive impedance as seen by the environment ensuring stable environment interactions.

The Rollett parameter K (Rollett, 1962) provides a means to test for absolute stability.

$$K = \frac{2\Re(Y_{11}(i\omega))\Re(Y_{22}(i\omega)) - \Re(Y_{12}(i\omega)Y_{21}(i\omega))}{|Y_{12}(i\omega)Y_{21}(i\omega)|} \tag{9}$$

Note that while this paper and the above expression use admittance parameters to model the slave robot and calculate K, the parameters $Y_{ij}(s)$ in the above expression can be replaced by the robot's corresponding impedance parameters $Z_{ij}(s)$ and the value of K remains the same.

For an LTI 2-port to be absolutely stable, it is necessary and sufficient for K to be greater than or equal to 1 at all frequencies and for both $Y_{11}(s)$ and $Y_{22}(s)$ to be positive real.

$$\begin{aligned} -90^\circ \leq \angle Y_{11}(i\omega) \leq 90^\circ \\ -90^\circ \leq \angle Y_{22}(i\omega) \leq 90^\circ \end{aligned} \tag{10}$$

Simplifying the analysis slightly, it has been noted that if $K \geq 1\ \forall\omega$ it is sufficient to only show that one of the admittances $Y_{11}(s)$ of $Y_{22}(s)$ is positive real as the other must be positive real as well (Meys, 1990).

2. Limitations of force control

The fundamental issue with force control, is that what it does and what it is often intended to do are not necessarily the same thing. Since inertial forces reduce the transparency of a slave robot, force control is often applied in an attempt to reduce the effective mass of the robot. Of course, part of the desire to reduce the effective mass of the robot is to reduce the impact forces that occur when the end-effector of the robot comes into contact with an external object. Unfortunately, since force control requires a measurement of external forces to determine the correct actuator torques, we run into a causality issue. We want to use force control to reduce impact forces, but force control cannot do anything about these impact forces until they have already occurred and been measured.

Limiting ourselves to LTI systems for the following analysis, this causality issue can be explained by and modeled as controller roll-off at high-frequencies. Since all force control algorithms are based on the desired force F_d, the measured environment force F_e, and the actuator velocity $\dot{x}_a$ (or position x_a), Figure 4 gives the most general 2-port block diagram that can be used to describe any particular force control algorithm. The open-loop robot admittance parameters are given by the transfer functions $R_{ij}(s)$, while $G_v(s)$, $G_{f_d}(s)$, and $G_{f_e}(s)$ represent the velocity feedback, force

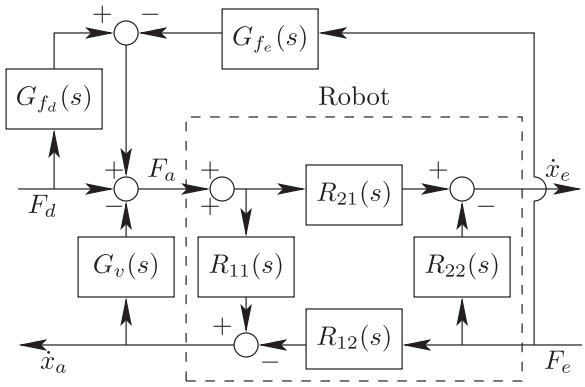

Fig. 4. Generalized 2-port block diagram for a force-controlled robot.

feed-forward, and force feedback transfer functions respectively. Solving for the closed-loop admittance parameters results in the following transfer functions:

$$
\begin{aligned}
Y_{11}(s) &= \left.\frac{\dot{x}_a(s)}{F_d(s)}\right|_{F_e=0} = \frac{R_{11}(s)\,(1+G_{f_d}(s))}{1+R_{11}(s)\,G_v(s)} \\
Y_{21}(s) &= \left.\frac{\dot{x}_e(s)}{F_d(s)}\right|_{F_e=0} = \frac{R_{21}(s)\,(1+G_{f_d}(s))}{1+R_{11}(s)\,G_v(s)} \\
Y_{12}(s) &= \left.\frac{\dot{x}_a(s)}{F_e(s)}\right|_{F_d=0} = \frac{R_{12}(s)+G_{f_e}(s)\,R_{11}(s)}{1+R_{11}(s)\,G_v(s)} \\
Y_{22}(s) &= \left.\frac{\dot{x}_e(s)}{F_e(s)}\right|_{F_d=0} = R_{22}(s) + \\
&\qquad \frac{R_{21}(s)\,[G_{f_e}(s)-R_{12}(s)\,G_v(s)]}{1+R_{11}(s)\,G_v(s)}
\end{aligned}
\tag{11}
$$

Since, as Eppinger and Seering (1987; 1992) pointed out, all controllers are fundamentally band limited due to unmodeled dynamics and roll-off in amplifiers and sensors. It is clear that at very high frequencies, the controllers $G_v(s)$, $G_{f_d}(s)$, and $G_{f_e}(s)$ must go to zero. Plugging in zero for these controllers in the above expressions shows unsurprisingly that the closed-loop admittance transfer functions $Y_{ij}(s)$ must match the admittance parameters of the open-loop robot at high-frequencies.

$$
Y_{ij}(s) \to R_{ij}(s) \quad \text{as} \quad s \to \infty \tag{12}
$$

The affect this roll-off has on the absolute stability of force controllers that attempt to reduce the effective inertia of the robot can be seen by studying the system's reflection admittances $R_{11}(s)$ and $R_{22}(s)$. Since all robots have some mass, and since inertial forces dominate at high-frequency, these reflected admittance transfer functions will always appear to be pure masses at high-frequencies with effective masses of M_{hf_a} and M_{hf_e} respectively. (Note, if the robot is rigid, $M_{hf_a} = M_{hf_e} = M$, where M is the mass of the robot; however, if there is any compliance in the robot this need not be true.) These open-loop admittance parameter transfer functions can therefore be approximated by:

$$
R_{11}(s) \to \frac{1}{M_{hf_a}s} \quad \text{and} \quad R_{22}(s) \to \frac{1}{M_{hf_e}s} \quad \text{as} \quad s \to \infty \tag{13}
$$

Combining the above two expressions, the closed-loop admittances $Y_{11}(s)$ and $Y_{22}(s)$ must also appear like pure masses at high-frequencies.

$$
\begin{aligned}
Y_{11}(s) \to R_{11}(s) \to \frac{1}{M_{hf_a}s} \quad &\text{and} \\
Y_{22}(s) \to R_{22}(s) \to \frac{1}{M_{hf_e}s} \quad &\text{as} \quad s \to \infty
\end{aligned}
\tag{14}
$$

While force control cannot affect the system's dynamics at high-frequencies, it can significantly alter the robot's closed-loop dynamics below the bandwidth of the force controller. Since the objective of force control is to increase the overall transparency of the robot, assume some force controller has been developed that achieves this increase in transparency by rejecting all the friction in the system and by making the robot appear to be a mass with mass M_{lf} at low frequencies, where M_{lf} is smaller than both M_{hf_a} and M_{hf_e}. The low-frequency reflection admittances are therefore given by:

$$
Y_{11}(s) = Y_{22}(s) \to \frac{1}{M_{lf}s} \quad \text{as} \quad s \to 0 \tag{15}
$$

Figure 5 plots a potential frequency response of $Y_{22}(s)$ for such a system. Note that at the bandwidth of the force controller, the controller is no longer able to modify the dynamics of the system and the magnitude of the frequency response must roll off as the system dynamics return to $\frac{1}{M_{hf_e}s}$. Since the high-frequency dynamics have a single pole at the origin, and therefore have a magnitude slope of -1 (-20 db/decade), the magnitude slope of $Y_{22}(s)$ must become steeper than -1 in order to return to the open-loop robot dynamics. According to Bode's gain–phase relationship, if the frequency response of $Y_{22}(s)$ is steeper than -1 over a reasonably large range of frequencies, then the phase of the transfer function must drop below -90° and the system violates the absolute stability requirement of (10).

In fact, it can be shown using Cauchy's Integral Theorem that this loss of phase, and the corresponding lack of absolute stability, occurs regardless of how the transition between the low- and high-frequency regimes happens. Even if the transition has very complicated dynamics the phase will always drop below -90° at some frequencies.

To start, the limitations on the locations of the poles and zeros in $Y_{22}(s)$ must be determined. Since both the low- and the high-frequency dynamics of $Y_{22}(s)$ have a slope of -1, $Y_{22}(s)$ must have a pole at the origin and be of relative degree 1. Therefore, aside from the pole at the origin,

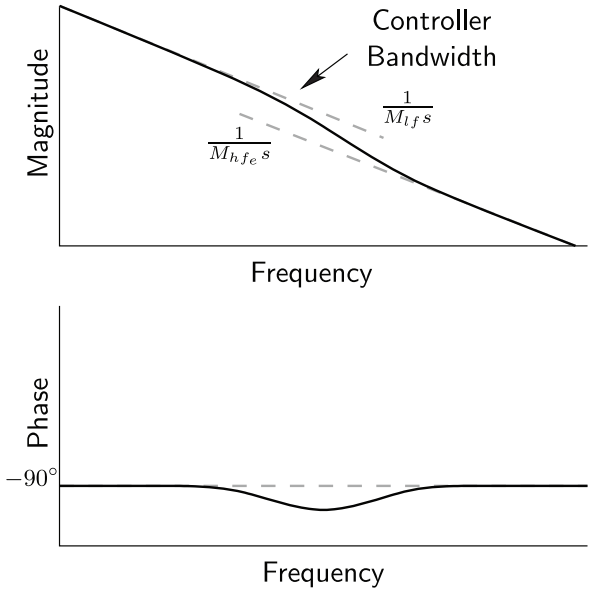

Fig. 5. Possible closed-loop frequency response of $Y_{22}(s)$ for a force controller that makes the robot appear to have a mass of M_{lf} below the bandwidth of the controller.

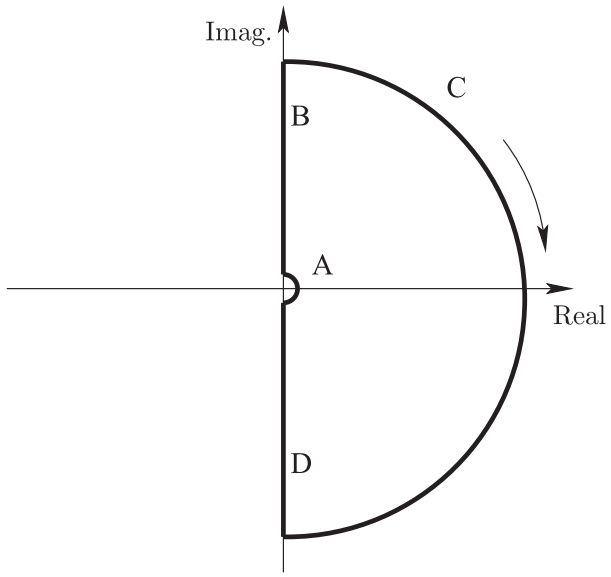

Fig. 6. Integration contour in complex plane.

$Y_{22}(s)$ must have an equal number of poles and zeros. Furthermore, if $Y_{22}(s)$ is to be positive real, all poles and zeros must be in the left half plane.

With no poles or zeros in the right half plane, Cauchy's Integral Theorem states that the integral of $Y_{22}(s)$ along the contour given in Figure 6, where the inner semi-circle is infinitely close to the origin and the outer semi-circle is infinitely far away from the origin, is equal to zero.

$$\begin{aligned}\oint Y_{22}(s)\,ds &= \int_A Y_{22}(s)\,ds + \int_B Y_{22}(s)\,ds \\ &\quad + \int_C Y_{22}(s)\,ds + \int_D Y_{22}(s)\,ds \\ &= 0\end{aligned} \tag{16}$$

For s infinitely close to zero $Y_{22}(s) = \frac{1}{M_{lf}s}$ and the integral along the inner semi-circle can be calculated by converting to polar coordinates ($s = R_i e^{i\theta}$ and $ds = iR_i e^{i\theta}\,d\theta$, where R_i is the radius of the infinitely small inner semi-circle).

$$\begin{aligned}\int_A Y_{22}(s)\,ds &= \int_A \frac{1}{M_{lf}s}ds \\ &= \int_{-\pi/2}^{\pi/2} \frac{iR_i e^{i\theta}}{M_{lf}R_i e^{i\theta}}d\theta = \frac{1}{M_{lf}}\pi i\end{aligned} \tag{17}$$

Similarly, for s infinitely large $Y_{22}(s) = \frac{1}{M_{hf_e}s}$ and the integral along the outer semi-circle with radius R_o becomes:

$$\begin{aligned}\int_C Y_{22}(s)\,ds &= \int_C \frac{1}{M_{hf_e}s}ds \\ = \int_{\pi/2}^{-\pi/2} \frac{iR_o e^{i\theta}}{M_{hf_e}R_o e^{i\theta}}d\theta &= -\frac{1}{M_{hf_e}}\pi i\end{aligned} \tag{18}$$

For the two components of the integral along the imaginary axis, the integral simply becomes the integral of i times the frequency response of $Y_{22}(s)$.

$$\begin{aligned}\int_B Y_{22}(s)\,ds &= \int_0^\infty iY_{22}(i\omega)\,d\omega \\ &\text{and} \\ \int_D Y_{22}(s)\,ds &= \int_{-\infty}^0 iY_{22}(i\omega)\,d\omega\end{aligned} \tag{19}$$

Since the imaginary part of $Y_{22}(i\omega)$ has odd symmetry, the integral of $\Im[Y_{22}(i\omega)]$ along the positive and negative parts of the imaginary axis cancel out. The real part of $Y_{22}(i\omega)$, on the other hand, has even symmetry so the integral of $\Re[Y_{22}(i\omega)]$ along each part of the axis is equal. Plugging the net contributions of the integral along each section of the contour into (16) and dividing through by i gives the following result.

$$\pi\left(\frac{1}{M_{lf}} - \frac{1}{M_{hf_e}}\right) + 2\int_0^\infty \Re\left[Y_{22}(i\omega)\right]d\omega = 0 \tag{20}$$

Since the apparent low-frequency mass of the system is smaller than the apparent high-frequency mass, $\frac{1}{M_{lf}} > \frac{1}{M_{hf_e}}$, and the first term in the above expression is a positive number. In order for the net integral to be zero, the second term must be a negative number. If the second term is negative however, the real part of $Y_{22}(i\omega)$ must be negative over some range of frequencies and $Y_{22}(s)$ cannot be positive real. The same argument can also be used to show the inability to increase the magnitude of $Y_{11}(s)$ above $\frac{1}{M_{hfa}s}$ while maintaining absolute stability.

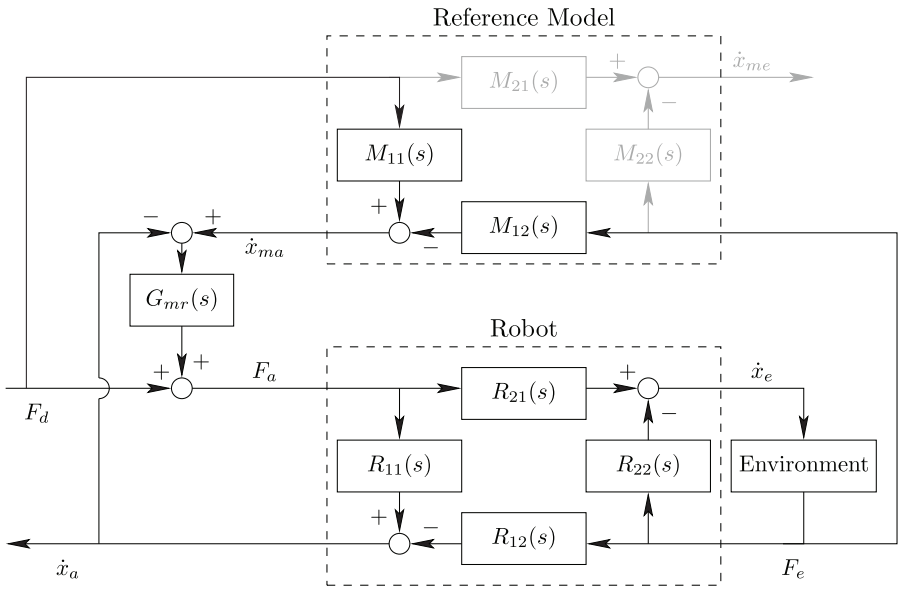

Fig. 7. 2-port block diagram for model-based force controller.

3. 2-port model-based force control for simple LTI systems

As the previous section showed, force control cannot hide a robot's inertia and maintain absolute stability. Therefore, the task of designing an absolutely stable force controller for a slave robot comes down to designing a controller that increases the admittance of the slave robot by rejecting friction and any unwanted damping. The model-based force control presented here achieves this friction rejection by providing the slave with an ideal, frictionless model of itself as reference. Both the desired and the measured environment forces are used to drive this reference model which provides the ideal velocity trajectory the robot would have in the absence of any joint friction. In turn, a velocity controller regulates the robot to follow this reference velocity.

While any useful controller must work on multi-DOF nonlinear robots, this section introduces model-based force control by focusing on a simplification of the more general controller which can be used with simple 1-DOF LTI robots. The hope is that by starting with this simplified version, the following analysis can help the reader develop a more intuitive understanding of the controller. The block-diagram in Figure 7 depicts the LTI version of model-based force control. Note that the model admittances $M_{21}(s)$ and $M_{22}(s)$ are only included here to depict the entire reference model and are not needed or used in the final control algorithm. The velocity controller is given by the transfer function $G_{mr}(s)$.

Using this model-based controller, the general expressions for the closed-loop admittances $Y_{ij}(s)$ are:

$$Y_{11}(s) = R_{11}(s)\,\frac{1 + M_{11}(s)\,G_{mr}(s)}{1 + R_{11}(s)\,G_{mr}(s)} \tag{21}$$

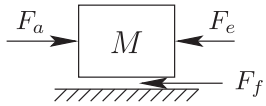

Fig. 8. Simple 1-DOF robot modeled as a mass subject to an applied actuator force F_a, an environment force F_e, and friction F_f.

$$Y_{21}(s) = R_{21}(s)\,\frac{1 + M_{11}(s)\,G_{mr}(s)}{1 + R_{11}(s)\,G_{mr}(s)} \tag{22}$$

$$Y_{12}(s) = R_{12}(s) + \frac{R_{11}(s)\,G_{mr}(s)\,(M_{12}(s) - R_{12}(s))}{1 + R_{11}(s)\,G_{mr}(s)} \tag{23}$$

$$Y_{22}(s) = R_{22}(s) + \frac{R_{21}(s)\,G_{mr}(s)\,(M_{12}(s) - R_{12}(s))}{1 + R_{11}(s)\,G_{mr}(s)} \tag{24}$$

Not surprisingly, if the robot and reference model match, i.e. if $R_{11}(s) = M_{11}(s)$ and $R_{12}(s) = M_{12}(s)$, then the controller does no work. Otherwise, as the gain of G_{mr} increases, the controller forces the actuator-side transfer functions Y_{11} and Y_{12} to match the reference model. The environment side admittance transfer functions Y_{22} and Y_{21} are modified similarly as G_{mr} increases, but due to the fact actuator forces cannot be immediately applied to the end-effector, the transformation may be limited by any internal dynamics within the robot.

Using the simple 1-DOF robot of Figure 8, and assuming the only friction on the robot is viscous friction ($F_f = b\dot{x}$) the open-loop robot admittances are given by:

$$R_{ij}(s) = \frac{1}{Ms + b} \tag{25}$$

To best match the rigid mass model of a robot considered here, the model should act as a reference mass M_r such that the admittances $M_{ij}(s)$ become:

$$M_{ij}(s) = \frac{1}{M_r s} \tag{26}$$

While there is significant freedom in selecting $G_{mr}(s)$, the work presented here focuses on the case where $G_{mr}(s)$ is a simple gain K_v representing proportional velocity control. More complex controllers may prove beneficial; however, care must be taken both to ensure the resulting system remains absolutely stable and to ensure sensor noise is not amplified. Plugging in these values for $R_{ij}(s)$, $M_{ij}(s)$, and $G_{mr}(s)$ the resulting admittance transfer functions, which are all identical since the robot is rigid, are given by:

$$Y_{ij}(s) = \frac{M_r s + K_v}{M_r s(Ms + (K_v + b))} \tag{27}$$

With all four admittance transfer functions identical, the Rollett parameter K from (9) is identically equal to 1 at all frequencies. The test for absolute stability therefore reduces to showing positive realness of $Y_{ij}(s)$ which turns out to be equivalent to showing that the closed-loop 2-port is passive. Noting the locations of the pole at $s = (K_v + b)/M$ and the zero at $s = K_v/M_r$, the phase of $Y_{ij}(s)$ stays between $\pm 90^\circ$ and the closed-loop system is absolutely stable as long as

$$M_r \geq M \frac{K_v}{K_v + b} \tag{28}$$

Since the viscous friction coefficient b is often only a very approximate model for the friction in the system a more conservative approach is to assume $b = 0$ and require

$$M_r \geq M \tag{29}$$

Figure 9 gives the frequency responses of $Y_{ij}(s)$ for the model-based force controller using M_r values that are both larger and smaller than M depicting the trade-off associated with choosing M_r. For the absolutely stable frequency response ($M_r > M$), the admittance $Y_{ij}(s)$ is greater than the open loop robot admittance $R_{ij}(s)$ at very low frequencies thanks to friction rejection, and comparable to $R_{ij}(s)$ at very high frequencies. For a frequency range in the middle, however, $R_{ij}(s)$ has a greater magnitude than $Y_{ij}(s)$. This indicates the force-controlled robot is actually less transparent than the open-loop robot across this frequency range. To make this range small, M_r should be chosen as close as possible to M such that it is still guaranteed to be greater than M once modeling error is accounted for.

In general, setting M_r to be as close to M as possible is desirable to minimize the mass the user will feel when using the telerobot. There are situations, however, where it may be beneficial to chose a larger model mass to improve the robustness of the controller. In particular, the analysis here assumes a rigid mass, but as pointed out in Eppinger and Seering (1992) real robots have structural compliance making force control a non-colocated control problem. When dealing with particularly compliant systems, with low natural frequencies, setting M_r to be large effectively reduces the bandwidth of the controller and can eliminate destabilizing high-frequency excitation. For further details, see Hart (2010) for a non-dimensional analysis showing the trade off between absolute stability and M_r for a 1-DOF robot with structural compliance.

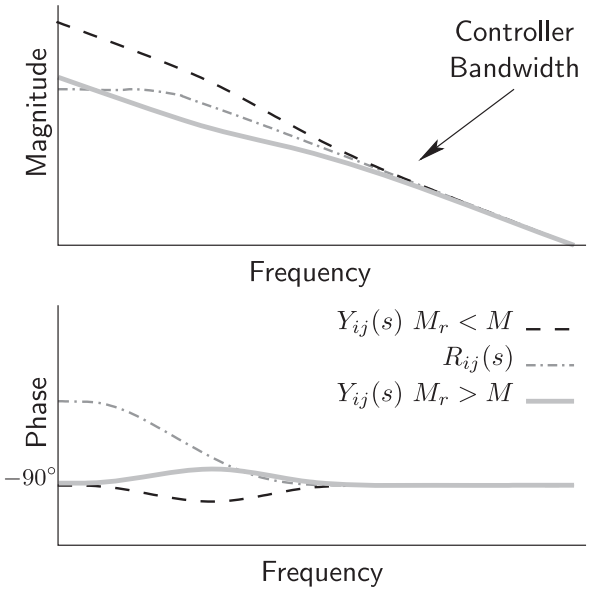

Fig. 9. Frequency response of closed loop admittances $Y_{ij}(s)$ for model-based force controller using both $M_r > M$ and $M_r < M$.

3.1. Energy storage function

While the model-based force controller is absolutely stable, it turns out that the controller is also passive as can be show using a Lyapunov like argument based on the Kalman–Yakubovich lemma. Additionally, in the process we will generate an energy storage function that will prove useful in showing passivity of the nonlinear multi-DOF version of the model-based controller in the following section.

The Kalman–Yakubovich lemma says that a stable linear system expressed in state space with state vector $\bar{x}$ and output y

$$\dot{\bar{x}} = A\bar{x} + Bu \qquad y = C\bar{x} \tag{30}$$

is passive with respect to the input u and the output y if

$$C = B^{\mathrm{T}}P \tag{31}$$

where P is the symmetric positive definite matrix that describes the energy V stored in the system (Slotine and Li, 1991).

$$V = \frac{1}{2}\bar{x}^{\mathrm{T}}P\bar{x} \tag{32}$$

Furthermore, the dissipation in the system is described by the symmetric positive semi-definite matrix Q

$$\dot{V} = -\frac{1}{2}\bar{x}^{\mathrm{T}} Q \bar{x} \tag{33}$$

which is related to P through the Lyapunov equation.

$$A^{\mathrm{T}} P + PA = -Q \tag{34}$$

Assuming a rigid robot such that $x_a = x_e = x$, the state vector for the model-based force controller contains the velocities of both the robot and the model $\bar{x} = [\dot{x}\ \dot{x}_m]^{\mathrm{T}}$. Continuing to model friction as viscous damping, the state space matrices are given by:

$$A = \begin{bmatrix} -\left(\frac{K_v}{M} + \frac{b}{M}\right) & \frac{K_v}{M} \\ 0 & 0 \end{bmatrix} \qquad B = \begin{bmatrix} \frac{1}{M} \\ \frac{1}{M_r} \end{bmatrix} \qquad C = \begin{bmatrix} 1 & 0 \end{bmatrix} \tag{35}$$

In order for $C = B^{\mathrm{T}} P$, P must take the form

$$P = \begin{bmatrix} M + P_{2,2}\frac{M^2}{M_r^2} & -P_{2,2}\frac{M}{M_r} \\ -P_{2,2}\frac{M}{M_r} & P_{2,2} \end{bmatrix} \tag{36}$$

where the $(2,2)$ element of P is as of yet unknown. Plugging P into the Lyapunov equation gives the following dissipation matrix.

$$\begin{aligned} Q &= \begin{bmatrix} Q_{1,1} & Q_{1,2} \\ Q_{2,1} & Q_{2,2} \end{bmatrix} \\ Q_{1,1} &= 2\left(K_v + b + (K_v + b) P_{2,2}\frac{M}{M_r^2}\right) \\ Q_{1,2} &= -\left(K_v + K_v P_{2,2}\frac{M}{M_r^2} + (K_v + b) P_{2,2}\frac{1}{M_r}\right) \\ Q_{2,1} &= -\left(K_v + K_v P_{2,2}\frac{M}{M_r^2} + (K_v + b) P_{2,2}\frac{1}{M_r}\right) \\ Q_{2,2} &= 2K_v P_{2,2}\frac{1}{M_r} \end{aligned} \tag{37}$$

For Q to be positive semi-definite, its determinant $(Q_{1,1}Q_{2,2} - Q_{1,2}Q_{2,1})$ must be greater than or equal to zero. Plugging the elements of Q into this expression, we find the expression is equal to zero, and has a global maximum at:

$$P_{2,2} = \frac{K_v M_r^2}{(K_v + b) M_r - K_v M} \tag{38}$$

Using this value for $P_{2,2}$, the energy storage matrix P becomes:

$$P = \begin{bmatrix} M + \frac{K_v M^2}{(K_v+b)M_r - K_v M} & -\frac{K_v M_r M}{(K_v+b)M_r - K_v M} \\ -\frac{K_v M_r M}{(K_v+b)M_r - K_v M} & \frac{K_v M_r^2}{(K_v+b)M_r - K_v M} \end{bmatrix} \tag{39}$$

The energy storage function $V = \frac{1}{2}\bar{x}^{\mathrm{T}} P \bar{x}$ can now be rewritten as

$$\begin{aligned} V =& \frac{1}{2} M \dot{x}^2 \\ &+ \frac{1}{2}\frac{K_v}{(K_v + b) M_r - K_v M}(M_r \dot{x}_m - M\dot{x})^2 \end{aligned} \tag{40}$$

Since the above expression is a sum of squared terms it is positive definite, and therefore a valid energy storage function as long as $M_r > M\frac{K_v}{K_v+b}$ (agreeing with the previous analysis). Note the storage function consists of two terms. The first represents the kinetic energy of the robot while the second represents the energy associated with the difference in momentum between the model and the robot.

To explore this idea of an energy term based on difference in momentum, imagine a frictionless ($b = 0$) 1-DOF robot under model-based force control that, starting from rest, experiences a rapidly applied force F at time $t = 0$ which can be approximated as an impulse I where $I = \int F\,dt$. Table 1 gives the momentum and velocity of both the robot and the model, as well as the kinetic energy of the robot and the total energy V in the system both immediately after the impulse was applied and at steady state once $\dot{x} = \dot{x}_m$.

Since both the robot and the model experience the same impulse, they both have the same momentum immediately after the impulse is applied. Equation (40) therefore tells us that V is equal to the kinetic energy of the robot. As time progresses, the model-based force controller will act to slow the robot until it approaches the velocity of the model. In doing so, the controller is reducing the kinetic energy of the robot without doing any work on the surrounding environment. In order to get this energy back at a later time, the controller stores most of this lost energy as a difference in momentum between the model and robot.

For this simple case with $b = 0$, equation (40) shows that the combination of the kinetic energy and the stored energy at steady state is actually equivalent to the kinetic energy of the model. Since energy is quadratic with velocity while momentum is only liner with velocity, yet both are linear with respect to mass, the kinetic energy of the model is always guaranteed to be less than the initial kinetic energy of the robot, and $V(t) \leq V(0^+)$ as required by passivity.

For the case where $b > 0$, equation (40) shows us the friction reduces the efficiency of the energy storage such that at steady state V will be less than the kinetic energy of the model with the exact amount depending on the ratio of K_v and b.

While equation (40) cannot be used to determine passivity when $M_r = M\frac{K_v}{K_v+b}$, since the Lyapunov function becomes unbounded, it is worth noting that this situation (which included the case of no friction and a perfect model) is still passive. To see this, set $M_r = M\frac{K_v}{K_v+b}$ in the equation of motion. After some simplification the equation of motion will reduce to the standard $M\ddot{x} = (F_d - F_e)$ and the energy storage function simply becomes the kinetic energy of the robot $V = \frac{1}{2}M\dot{x}^2$.

3.2. Integral control interpretation

Noting that the desired and measured environment forces run through the model, and since the model of the robot takes the form $\frac{1}{M_r s}$ it is unsurprising to discover that the

Table 1. Momentum, velocity, kinetic energy, and total energy V for a frictionless ($b = 0$) robot under model-based force control both immediately after an applied impulse of I and at steady state.

	Robot momentum	Robot velocity	Model momentum	Model velocity	Robot kinetic energy	Total energy (V)
Immediately after impulse	I	$\frac{I}{M}$	I	$\frac{I}{M_r}$	$\frac{1}{2M}I^2$	$\frac{1}{2M}I^2$
Steady state	$\frac{M}{M_r}I$	$\frac{I}{M_r}$	I	$\frac{I}{M_r}$	$\frac{1}{2}M\left(\frac{I}{M_r}\right)^2$	$\frac{1}{2M_r}I^2$

model-based force control achieves perfect steady state force tracking as the model acts like an integral control term. Integral control is quite common in direct force controllers because it provides perfect force tracking at low frequencies. Despite the benefits, several studies have made clear the need for additional stabilization when using integral terms on force error. Nonlinear anti-windup methods have proven useful in eliminating issues cause by controller saturation in Wilfinger et al. (1994). A parallel force controller combining a P.D. position controller with a P.I. force controller resulted in a stable force controller in Chiaverini et al. (1994). Similarly, Xu et al. (2000) showed enhanced stability of integral force controllers when using velocity and acceleration feedback to help dampen out oscillation.

In model-based control, choosing $M_r > M$ automatically ensures enough damping is added to the system to stabilize the integral action. Placing the model-based force controller in the general form of Figure 4 results in the following generalized controllers $G_{fd}(s)$, $G_{fe}(s)$, and $G_v(s)$.

$$G_{fd}(s) = G_{fe}(s) = \frac{K_v}{M_r s} \qquad \text{and} \qquad G_v(s) = K_v \tag{41}$$

and a control law of:

$$F_c = F_d + \frac{K_v}{M_r s}(F_d - F_e) - K_v \dot{x} \tag{42}$$

This controller represents feed-forward control of F_d, integral control on force error with a gain of $K_i = \frac{K_v}{M_r}$, and added viscous damping with a gain of K_v to help stabilize the system.

3.3. Robustness to Coulomb friction

So far, the friction the model-based force controller is designed to reject has been modeled as viscous damping. To be useful however, model-based force control must maintain absolute stability when subject to more realistic non-linear friction forces such as Coulomb friction.

To show passivity in the presence of Coulomb friction, we first examine the equations of motion that describe the system. The reference model's equation of motion is given by:

$$M_r \ddot{x}_m = F_d - F_e \tag{43}$$

Since the model velocity $\dot{x}_m$ represents the ideal velocity of the robot in the absence of friction and other disturbance forces, the velocity controller $G_{mr}(s) = K_v$ develops a control force F_c implemented to make the robot follow the model velocity.

$$F_c = K_v(\dot{x}_m - \dot{x}) \tag{44}$$

The resulting equation of motion for the robot then becomes

$$M\ddot{x} = (F_d - F_e) + (F_c - F_f) \tag{45}$$

where $(F_d - F_e) = F_{\text{ext}}$ is the net external force acting on the robot and $(F_c - F_f)$ is the residual disturbance after the force control is applied.

To show passivity of this model-based force controller we must verify that the residual disturbance is passive. First examine the dynamics of F_c. Subtracting (45) from (43) followed by subtracting $M_r\ddot{x}$ from both sides of the equation results in the following LTI differential equation for the control force F_c.

$$\frac{M_r}{K_v}\dot{F}_c + F_c = F_f - (M_r - M)\ddot{x} \tag{46}$$

The above expression shows the control force is simply a low-passed version of the sum of the friction force F_f and an inertial force $(M_r - M)\ddot{x}$ arising from the difference in the model and robot masses.

Assuming the friction on the robot consists of both viscous and Coulomb friction forces, the friction force F_f can be expressed as:

$$F_f = F_{fv} + F_{fc} \qquad \text{where}$$
$$F_{fv} = b\dot{x} \qquad \text{and} \qquad F_{fc} = C\,\text{sgn}(\dot{x}) \tag{47}$$

Since (46) is LTI, superposition holds and the control force can be viewed as the summation of three separate control forces arising to compensate for both types of friction and the inertial force arising from the mass difference.

$$F_c = F_{cv} + F_{cc} + F_{cm} \tag{48}$$

Now each control force can be expressed in terms of the LTI differential equation from above.

$$\frac{M_r}{K_v}\dot{F}_{cv} + F_{cv} = F_{fv} \tag{49}$$

$$\frac{M_r}{K_v}\dot{F}_{cc} + F_{cc} = F_{fc} \tag{50}$$

$$\frac{M_r}{K_v}\dot{F}_{cm} + F_{cm} = -(M_r - M)\ddot{x} \tag{51}$$

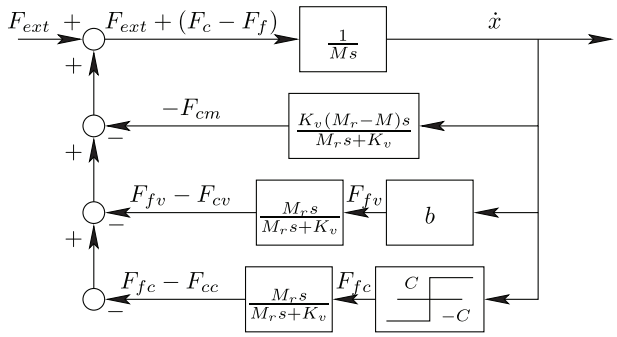

Fig. 10. Block diagram showing passivity of 1-DOF model-based force control.

Since the control forces are low-pass filtered versions of the friction forces the above expressions can be thought of as disturbance estimators for the friction forces. After applying our estimate of the disturbances the residual friction forces, $F_{fv} - F_{cv}$ and $F_{fc} - F_{cc}$, become high-passed versions of the friction forces.

$$F_{f(v,c)} - F_{c(v,c)} = \left[1 - \frac{K_v}{M_r s + K_v}\right] F_{f(v,c)} = \frac{M_r s}{M_r s + K_v} F_{f(v,c)} \tag{52}$$

Using these expressions combined with (51) the system can now be expressed by the block diagram of Figure 10.

Since this block diagram representation of the closed-loop robot consists of a 1-port representation of the robot connected in feedback with three 1-port systems, we need only show that the 1-port robot and each of the three 1-port systems in feedback are passive to prove that the entire system is passive.

As mentioned in Section 1, for a linear 1-port systems to be passive, the phase of its transfer function must always be between $\pm 90^\circ$. From this we immediately see that both the robot and the system representing the viscous friction and its compensation are passive.

$$G_{\text{robot}}(s) = \frac{1}{Ms} \tag{53}$$

$$G_{\text{viscous}}(s) = b\frac{M_r s}{M_r s + K_v} \tag{54}$$

Furthermore if we stipulate that $M_r \geq M$, as required by previous analysis, the system representing the control force arising from the difference in the model and robot masses is also passive.

$$G_{\text{inertia}}(s) = (M_r - M)\frac{K_v s}{M_r s + K_v} \tag{55}$$

This leaves only the system which describes the Coulomb friction and its compensation. Since Coulomb friction is inherently non-linear we must explicitly examine the net power flow into the system.

$$\int \dot{x}(F_{fc} - F_{cc})\, dt \tag{56}$$

For any given non-zero velocity $\dot{x}$ the Coulomb friction force F_{fc} must be either C or $-C$ corresponding to the sign of the velocity. Since F_{cc} is a low-passed version of F_{fc} we can bound F_{cc}.

$$|F_{cc}| \leq C \tag{57}$$

Combining the two forces we see that

$$0 \leq F_{fc} - F_{cc} \leq 2C \quad \text{for} \quad \dot{x} > 0 \tag{58}$$

$$-2C \leq F_{fc} - F_{cc} \leq 0 \quad \text{for} \quad \dot{x} < 0 \tag{59}$$

which implies

$$(F_{fc} - F_{cc})\dot{x} \geq 0 \tag{60}$$

Thus the integral of (56) is always positive, indicating a passive system and completing the analysis showing model-based force control to be passive in 1-DOF in the presence of Coulomb friction.

While friction in general includes many other nonlinear terms which have been neglected in the above analysis, viscous and Coulomb friction often represent the majority of the disturbance forces. As such, showing passivity with respect to these two friction forces indicates model-based force control will be very robust in practice.

4. Multi-DOF model based force control

The only real difference between the full multi-DOF controller presented in this section and the simplified 1-DOF controller from the previous section is that the model used to provide the robot with its ideal velocity trajectory is more complex. Once this model is known however, applying model-based force control is quite simple.

Multi-DOF robots are typically modeled using the full Euler–Lagrangian equations of motion. Assuming gravitational forces have been compensated for, the equations of motion for a n-DOF robot are given by:

$$\boldsymbol{M}(q)\ddot{q} + \boldsymbol{C}(q, \dot{q})\dot{q} = \tau_d + \tau_c - \tau_f - \tau_e \tag{61}$$

where $q \in \mathbb{R}^n$ is the vector of joint positions, $\boldsymbol{M}(q) \in \mathbb{R}^{n \times n}$ is the symmetric and positive definite mass matrix, $\boldsymbol{C}(q, \dot{q}) \in \mathbb{R}^{n \times n}$ is the matrix of centripetal and Coriolis forces, and τ_d, τ_c, τ_f, and τ_e represent the generalized desired, controller, friction, and environmental forces respectively.

Based on these equations of motion, the ideal frictionless reference model used to provide the reference velocity in the model-based control framework will take the following form

$$\boldsymbol{M}_r(q)\ddot{q}_m + \boldsymbol{C}_r(q, \dot{q})\dot{q}_m = \tau_d - \tau_e \tag{62}$$

where $\boldsymbol{M}_r(q)$ is the model's mass matrix and $\boldsymbol{C}_r(q, \dot{q})$ is the model's centripetal and Coriolis matrix. For the model to be passive, $\boldsymbol{M}_r(q)$ must be symmetric and positive definite for all values of q, and $\dot{\boldsymbol{M}}_r$, the time derivative of $\boldsymbol{M}_r(q)$, must equal $\boldsymbol{C}_r + \boldsymbol{C}_r^{\mathrm{T}}$.

Note that for the model to accurately capture the inertial properties of the robot, $\boldsymbol{M}_r(q)$ and $\boldsymbol{C}_r(q, \dot{q})$ must be defined

in terms of the robot's position q and velocity $\dot{q}$ and not the model states q_m and $\dot{q}_m$.

As in the 1-DOF case, simulating the model using τ_d and τ_e as the inputs produces the model velocity vector $\dot{q}_m$. This velocity vector represents the ideal joint velocities the robot would have at any given moment based on its position, velocity, and applied external torques if friction forces were not present.

Once $\dot{q}_m$ is calculated, a velocity controller drives the robot to match the model joint velocities using a positive definite gain matrix $\boldsymbol{K}_v$.

$$\tau_c = \boldsymbol{K}_v(\dot{q}_m - \dot{q}) \tag{63}$$

The resulting control algorithm is depicted by the block diagram of Figure 11. Note that for simplicity, in the following analysis and in the experimental results of the following section, $\boldsymbol{K}_v$ is set to be a diagonal matrix $K_v I$ where I is the $n \times n$ identity matrix and K_v is a scalar gain value.

4.1. Multi-DOF passivity analysis

To check for passivity of the multi-DOF model-based force controller we can start with the energy storage function developed in Section 3. First let $\boldsymbol{M_r} - \boldsymbol{M} = \tilde{\boldsymbol{M}}$ where $\boldsymbol{M_r}$ is chosen such that $\tilde{\boldsymbol{M}}$ is positive definite ($\boldsymbol{M_r} > \boldsymbol{M}$) to avoid attempting to hide any inertial forces. Ignoring the viscous friction terms, the storage function (40) can be rewritten in terms of the multi-DOF state vector $\bar{q} = [\dot{q}^{\mathrm{T}}\ \dot{q}_m^{\mathrm{T}}]^{\mathrm{T}}$.

$$V = \frac{1}{2}\bar{q}^{\mathrm{T}} P \bar{q} \tag{64}$$

$$V = \frac{1}{2}\begin{bmatrix}\dot{q}^{\mathrm{T}} & \dot{q}_m\end{bmatrix}\begin{bmatrix}\boldsymbol{M} + \boldsymbol{M}\tilde{\boldsymbol{M}}^{-1}\boldsymbol{M} & -\boldsymbol{M}\tilde{\boldsymbol{M}}^{-1}\boldsymbol{M_r} \\ -\boldsymbol{M_r}\tilde{\boldsymbol{M}}^{-1}\boldsymbol{M} & \boldsymbol{M_r}\tilde{\boldsymbol{M}}^{-1}\boldsymbol{M_r}\end{bmatrix}\begin{bmatrix}\dot{q} \\ \dot{q}_m\end{bmatrix}$$

For the multi-DOF algorithm to be passive, the change in the stored energy in the system must be expressed in term of $\dot{V} = \dot{q}^{\mathrm{T}}\tau_{\mathrm{ext}} - f(\bar{q})$ where $\tau_{\mathrm{ext}} = \tau_d - \tau_e$ such that $\dot{q}^{\mathrm{T}}\tau_{\mathrm{ext}}$ represents the net power flow into the closed-loop system and $f(\bar{q})$ is some positive semi-definite dissipation function.

Taking the derivative with respect to time of the energy storage function yields

$$\dot{V} = \bar{q}^{\mathrm{T}} P \dot{\bar{q}} + \frac{1}{2}\bar{q}^{\mathrm{T}}(R + R^{\mathrm{T}})\bar{q} \tag{65}$$

where $\dot{P} = R + R^{\mathrm{T}}$. Letting $\tilde{\boldsymbol{C}} = \boldsymbol{C}_r - \boldsymbol{C}$ such that $\dot{\tilde{\boldsymbol{M}}} = \tilde{\boldsymbol{C}} + \tilde{\boldsymbol{C}}^{\mathrm{T}}$ and substituting $\dot{\boldsymbol{M}} = \boldsymbol{C} + \boldsymbol{C}^{\mathrm{T}}$, and $\dot{\boldsymbol{M}}_r = \boldsymbol{C}_r + C_r^{\mathrm{T}}$, the matrix R after some algebra can be expressed as:

$$R = \begin{bmatrix}R_{1,1} & R_{1,2} \\ R_{2,1} & R_{2,2}\end{bmatrix} \tag{66}$$

where

$$R_{1,1} = \boldsymbol{C} + \boldsymbol{C}\tilde{\boldsymbol{M}}^{-1}\boldsymbol{M} - \boldsymbol{M}\tilde{\boldsymbol{M}}^{-1}\tilde{\boldsymbol{C}}\tilde{\boldsymbol{M}}^{-1}\boldsymbol{M} + \boldsymbol{M}\tilde{\boldsymbol{M}}^{-1}\boldsymbol{C} \tag{67}$$

$$R_{1,2} = -\left(\boldsymbol{C}\tilde{\boldsymbol{M}}^{-1}\boldsymbol{M_r} - \boldsymbol{M}\tilde{\boldsymbol{M}}^{-1}\tilde{\boldsymbol{C}}\tilde{\boldsymbol{M}}^{-1}\boldsymbol{M_r} + \boldsymbol{M}\tilde{\boldsymbol{M}}^{-1}\boldsymbol{C_r}\right) \tag{68}$$

$$R_{2,1} = -\left(\boldsymbol{C_r}\tilde{\boldsymbol{M}}^{-1}\boldsymbol{M} - \boldsymbol{M_r}\tilde{\boldsymbol{M}}^{-1}\tilde{\boldsymbol{C}}\tilde{\boldsymbol{M}}^{-1}\boldsymbol{M} + \boldsymbol{M_r}\tilde{\boldsymbol{M}}^{-1}\boldsymbol{C}\right) \tag{69}$$

$$R_{2,2} = \boldsymbol{C_r}\tilde{\boldsymbol{M}}^{-1}\boldsymbol{M_r} - \boldsymbol{M_r}\tilde{\boldsymbol{M}}^{-1}\tilde{\boldsymbol{C}}\tilde{\boldsymbol{M}}^{-1}\boldsymbol{M_r} + \boldsymbol{M_r}\tilde{\boldsymbol{M}}^{-1}\boldsymbol{C_r} \tag{70}$$

The robot and model equations of motion as well as the control torque expression $\tau_c = \boldsymbol{K}_v(\dot{q}_m - \dot{q})$ can be substituted into the term $\bar{q}^{\mathrm{T}} P \dot{\bar{q}}$ in $\dot{V}$.

$$\begin{aligned}\dot{V} = {} & \dot{q}^{\mathrm{T}}\tau_{\mathrm{ext}} + \bar{q}^{\mathrm{T}}\begin{bmatrix}-\boldsymbol{C} - \boldsymbol{M}\tilde{\boldsymbol{M}}^{-1}\boldsymbol{C} & \boldsymbol{M}\tilde{\boldsymbol{M}}^{-1}\boldsymbol{C_r} \\ \boldsymbol{M_r}\tilde{\boldsymbol{M}}^{-1}\boldsymbol{C} & \boldsymbol{M_r}\tilde{\boldsymbol{M}}^{-1}\boldsymbol{C_r}\end{bmatrix}\bar{q} \\ & - \bar{q}^{\mathrm{T}}\begin{bmatrix}\boldsymbol{M}\tilde{\boldsymbol{M}}^{-1}\boldsymbol{K_v} + \boldsymbol{K_v} & -\boldsymbol{M}\tilde{\boldsymbol{M}}^{-1}\boldsymbol{K_v} - \boldsymbol{K_v} \\ -\boldsymbol{M_r}\tilde{\boldsymbol{M}}^{-1}\boldsymbol{K_v} & \boldsymbol{M_r}\tilde{\boldsymbol{M}}^{-1}\boldsymbol{K_v}\end{bmatrix}\bar{q} \\ & + \frac{1}{2}\bar{q}^{\mathrm{T}}(R + R^{\mathrm{T}})\bar{q}\end{aligned} \tag{71}$$

The third term in the above expression, while not symmetric, is a positive semi-definite quadratic dissipation function. The first and third terms therefore represent the desired result. Furthermore, comparing the second term with the expressions for the elements in R it can be seen that if

$$\boldsymbol{C} = \boldsymbol{M}\tilde{\boldsymbol{M}}^{-1}\tilde{\boldsymbol{C}} \qquad \text{and} \qquad \boldsymbol{C}_r = \boldsymbol{M}_r\tilde{\boldsymbol{M}}^{-1}\tilde{\boldsymbol{C}} \tag{72}$$

then the fourth term $\frac{1}{2}\bar{q}^{\mathrm{T}}(R + R^{\mathrm{T}})\bar{q}$ simplifies to cancel the second term. Expressing the dissipation function in terms of its symmetric component $Q = \frac{1}{2}(L + L^{\mathrm{T}})$, where L is the matrix from the dissipation function as seen above, the final expression for $\dot{V}$ becomes:

$$\dot{V} = \dot{q}^{\mathrm{T}}\tau_{\mathrm{ext}} - \bar{q}^{\mathrm{T}}\begin{bmatrix}Q_{1,1} & Q_{1,2} \\ Q_{2,1} & Q_{2,2}\end{bmatrix}\bar{q} \tag{73}$$

where Q is positive semi-definite and

$$Q_{1,1} = \frac{1}{2}\left(\boldsymbol{M}\tilde{\boldsymbol{M}}^{-1}\boldsymbol{K_v} + \boldsymbol{K_v}\tilde{\boldsymbol{M}}^{-1}\boldsymbol{M}\right) + \boldsymbol{K_v} \tag{74}$$

$$Q_{1,2} = -\frac{1}{2}\left(\boldsymbol{M}\tilde{\boldsymbol{M}}^{-1}\boldsymbol{K_v} + \boldsymbol{K_v}\tilde{\boldsymbol{M}}^{-1}\boldsymbol{M_r}\right) - \frac{1}{2}\boldsymbol{K_v} \tag{75}$$

$$Q_{2,1} = -\frac{1}{2}\left(\boldsymbol{M_r}\tilde{\boldsymbol{M}}^{-1}\boldsymbol{K_v} + \boldsymbol{K_v}\tilde{\boldsymbol{M}}^{-1}\boldsymbol{M_r}\right) - \frac{1}{2}\boldsymbol{K_v} \tag{76}$$

$$Q_{2,2} = \frac{1}{2}\left(\boldsymbol{M_r}\tilde{\boldsymbol{M}}^{-1}\boldsymbol{K_v} + \boldsymbol{K_v}\tilde{\boldsymbol{M}}^{-1}\boldsymbol{M_r}\right) \tag{77}$$

which completes the passivity proof.

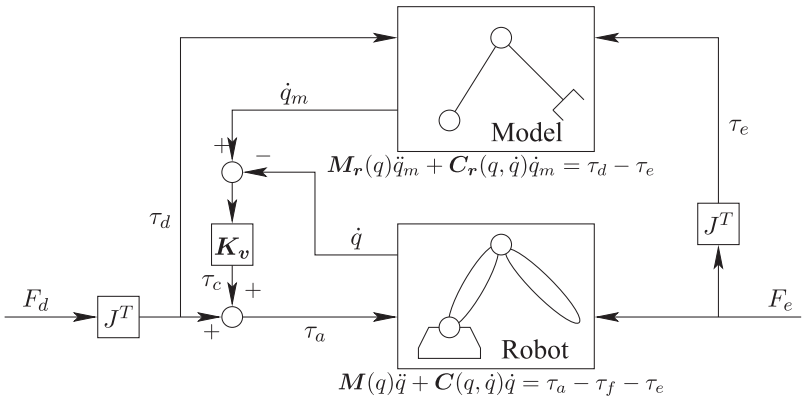

Fig. 11. Multi-DOF model-based force controller.

For the above proof to be valid the expressions in (72) had to be true in order for the energy storage terms that depended on the time derivatives of $\boldsymbol{M}$ and $\boldsymbol{M_r}$ to cancel out. Combining these expressions results in the following criterion on $\boldsymbol{C_r}$.

$$\boldsymbol{C_r} = \boldsymbol{M_r}\boldsymbol{M}^{-1}\boldsymbol{C} \tag{78}$$

Additionally, as mentioned above, $\boldsymbol{M_r}$ and $\boldsymbol{C_r}$ must represent passive dynamics which requires:

$$\dot{\boldsymbol{M}}_{\boldsymbol{r}} = \boldsymbol{C_r} + \boldsymbol{C}_{\boldsymbol{r}}^{\mathrm{T}} = \boldsymbol{M_r}\boldsymbol{M}^{-1}\boldsymbol{C} + \boldsymbol{C}^{\mathrm{T}}\boldsymbol{M}^{-1}\boldsymbol{M_r} \tag{79}$$

After examining the above expression it appears that if the model mass matrix and centripetal and Coriolis matrix are chosen to be scaled versions of the robot's parameters

$$\boldsymbol{M_r} = (1+\epsilon)\,\boldsymbol{M} \quad \text{and} \quad \boldsymbol{C_r} = (1+\epsilon)\,\boldsymbol{C} \quad \text{for} \quad \epsilon > 0 \tag{80}$$

then $\boldsymbol{M_r}\boldsymbol{M}^{-1} = (1+\epsilon)$, and the derivative of the model mass matrix is $\dot{\boldsymbol{M}}_{\boldsymbol{r}} = (1+\epsilon)\,\boldsymbol{C} + (1+\epsilon)\,\boldsymbol{C}^{\mathrm{T}} = \boldsymbol{C_r} + \boldsymbol{C}_{\boldsymbol{r}}^{\mathrm{T}}$. Having met the above criterion, the resulting system is guaranteed to be passive.

The above result is quite powerful in that it shows that a passive multi-DOF model-based force control can be built. In actual implementations however, passivity may not be achievable as it will be almost impossible to exactly meet the conditions in (80) due to errors in estimating $\boldsymbol{M}$ and $\boldsymbol{C}$.

Noting however that the criterion in (79) arises from the need to keep the actual and model centripetal and Coriolis forces pointed in the same direction we see that developing a model that exactly matches (80) may not be all that important. Since these forces represent second order dynamics, they are typically quite small if the robot is moving at reasonable speeds and are nonexistent when the robot is stationary.

Neglecting the centripetal and Coriolis forces by setting $\boldsymbol{C} = 0$ and $\boldsymbol{C_r} = 0$ and differentiating the energy storage function $\frac{1}{2}\bar{q}^{\mathrm{T}}P\bar{q}$ directly leads to the dissipation function $\dot{V} = \dot{q}^{\mathrm{T}}\tau_{\mathrm{ext}} - \bar{q}^{\mathrm{T}}Q\bar{q}$. As this matches the dissipation function from before we see that to the first order the model reference force controller is passive as long as $\boldsymbol{M_r} > \boldsymbol{M}$. Said another way, as long as the effective inertia of the model is always greater then the effective inertia of the robot in every direction then small differences in the direction and magnitude of the centripetal and Coriolis forces will typically be negligible.

5. Using model based force control in telerobotics

Since model-based force control results in a passive 2-port slave system there is little concern that excess energy generated by the slave-side force control can destabilize a lager telerobotic system. As such, slave robots using model-based force control fit quite nicely into the established telerobotic control architectures.

To compare various telerobotic control architectures with and without the use of model-based force control around the slave, a simple telerobotic system was set up using a 2-DOF planar robotic arm as the slave device and a Phantom haptic device as master as shown in Figure 12. With encoders on both the slave device and the Phantom, and a 6-DOF force/torque sensor at the end-effector of the slave, the resulting system can be configured to run any telerobotic controller that utilizes measurements of master position, slave position, and environment force. The telerobotic system is controlled using a PC running real-time Linux executing a 1 kHz servo loop.

To approximate an industrial like robot, the slave robot's two motors both have a gear ratio of 113 : 1 resulting in significant internal friction. The robot's inertial parameters were estimated using a system-identification analysis and are provided in Table 2. The robot's geometric properties are defined as shown in Figure 13.

The complete Lagrangian model of the 2-DOF slave is represented by its Jacobian,

$$J = \begin{bmatrix} -l_1 \sin(q_1) - l_2 \sin(q_1+q_2) & -l_2 \sin(q_1+q_2) \\ l_1 \cos(q_1) + l_2 \sin(q_1+q_2) & l_2 \cos(q_1+q_2) \end{bmatrix} \tag{81}$$

its mass matrix,

$$\boldsymbol{M} = \begin{bmatrix} m_{1,1} & m_{1,2} \\ m_{2,1} & m_{2,2} \end{bmatrix} \tag{82}$$

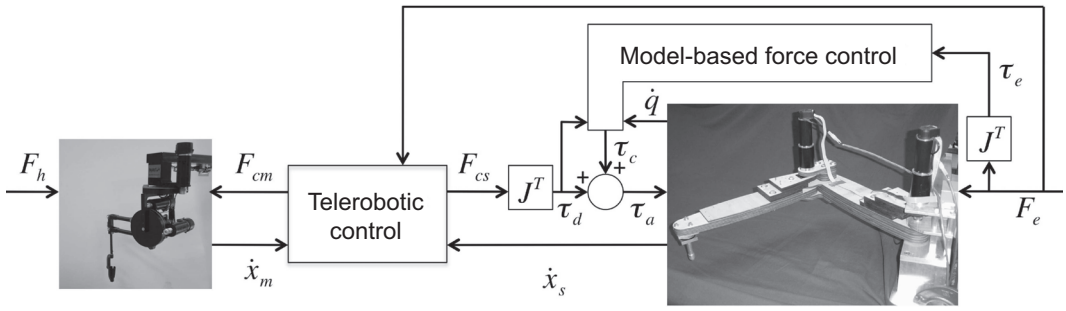

Fig. 12. Telerobotic system used to compare performance of various teleoperation control architectures with and without model-based force control.

Table 2. Parameters of 2-DOF planar mechanism.

Parameter	Symbol	Value
Link 1 mass	m_1	2.328 kg
Link 2 mass	m_2	0.939 kg
Link 1 inertia	I_1	0.057 kgm^2
Link 2 inertia	I_2	0.020 kgm^2
Joint 1 motor inertia	I_{m_1}	7.021×10^{-6} kgm^2
Joint 2 motor inertia	I_{m_2}	7.021×10^{-g} kgm^2
Link 1 length	l_1	0.350 m
Link 2 length	l_2	0.350 m
Radial distance to link 1 center of mass	r_1	0.235 m
Radial distance to link 2 center of mass	r_2	0.171 m

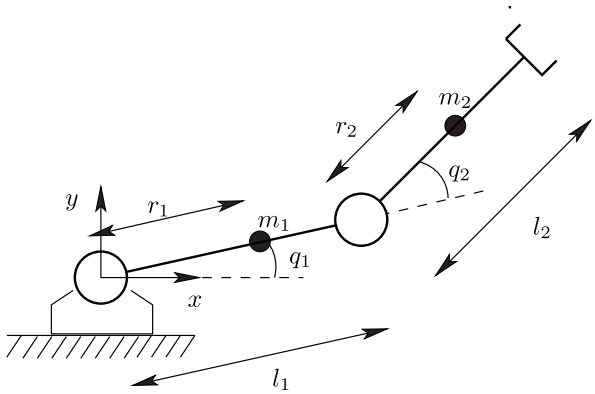

Fig. 13. Geometric definitions for 2-DOF mechanism.

where

$$m_{1,1} = m_r r_1^2 + I_1 + \eta^2 I_{m_1} + I_{m_2} + m_2(l_1^2 + r_2^2 + 2l_1 r_2 \cos(q_2)) \quad (83)$$

$$m_{1,2} = I_2 + \eta I_{m_2} + m_2(r_2^2 + l_1 r_2 \cos(q_2)) \quad (84)$$

$$m_{2,1} = I_2 + \eta I_{m_2} + m_2(r_2^2 + l_1 r_2 \cos(q_2)) \quad (85)$$

$$m_{2,2} = I_2 + \eta^2 I_{m_2} + m_2 r_2^2 \quad (86)$$

and its centripetal and Coriolis matrix.

$$\boldsymbol{C} = \begin{bmatrix} -m_2 l_1 r_2 \sin(q_2)\dot{q}_2 & -m_2 l_1 r_2 \sin(q_2)(\dot{q}_1 + \dot{q}_2) \\ m_2 l_1 r_2 \sin(q_2)\dot{q}_1 & 0 \end{bmatrix} \quad (87)$$

Note that η is used here to represents the gear ratio of the robot's motors.

Due to the kinematic dissimilarity between the master and slave devices, the telerobotic controllers are implemented in Cartesian space and the applied forces are converted to joint torques using the transpose of each robot's Jacobian matrix. Additionally, since the Phantom is a 3-DOF device, only the Phantom's position in the horizontal plane is sent to the telerobotic controller and the Phantom is allowed to float uncontrolled in the vertical direction.

For the two telerobotic controllers studied here, the position–position controller and a modified 4-channel controller, adding model-based force control around the slave was as simple as setting the slave-side controller force F_{cs} calculated by the telerobotic controller to be the desired force input given to the model-based controller. For both cases, the model mass matrix $\boldsymbol{M_r}$ and centripetal and Coriolis matrix $\boldsymbol{C_r}$ were set to be $1.01\boldsymbol{M}$ and $1.01\boldsymbol{C}$ respectively, while the model-based velocity control gain K_v was set to be 30 Nms/rad.

To experimentally explore the transparency and robustness of the telerobotic systems both with and without model-based force control, a human operator, holding on to the Phantom device, drove the slave through free-space along the negative x-direction until it made contact with either a block of foam or a stiff aluminum block. Upon making contact, the user then tried to maintain an approximately constant contact force at the remote environment until the completion of the 5 s experiment.

5.1. Position-position control

The position–position telerobotic controller consists of two identical position controllers driving the master and slave to track each other. The resulting controller is very robust at the cost of poor transparency. Using PD position controllers provides the following control algorithm:

$$\begin{aligned} F_{cs} &= K_p(x_m - x_s) + K_d(\dot{x}_m - \dot{x}_s) \\ F_{cm} &= -K_p(x_m - x_s) - K_d(\dot{x}_m - \dot{x}_s) \end{aligned} \quad (88)$$

Here the control forces on master, F_{cm}, and slave, F_{cs}, are equal and opposite, and the resulting controller is passive. Using this passive position–position controller to connect a passive master with a passive slave results in a string of passive 2-port elements, the combination of which will be stable for all possible environments and human impedances.

As the position–position controller makes no attempt to hide the master or slave dynamics from the user, it results in a system that feels heavy in free-space. Furthermore, the bilateral position controllers of (88) can be viewed as connecting the end-effectors of the master and slave together using a virtual spring and damper. Due to this virtual coupling, the maximum stiffness the user will ever feel is K_p regardless of the actual environment stiffness.

For the system considered here K_p was set to 200 N/m and K_d was set to 6 Ns/m. Note that this value for K_d is quite small resulting in a highly undamped system. Unfortunately this was the maximum value that could be used before quantization noise in the velocity estimate of the master device and other such non-idealities caused the Phantom to buzz uncontrollably.

In addition to the relatively high effective inertia and low stiffness, the virtual spring and damper effectively low-pass filters the forces being transmitted from user to environment and vice versa. Without being able to feel the high-frequency component of impact forces it is quite difficult for the operator to detect the exact moment of impact. Similarly it is impossible to develop any kind of feel for the surface texture of the remote environment.

5.1.1. Impact experiments Figure 14 gives the environment force F_e, the negative of the control force at the master $-F_{cm}$, the slave position x_s, and the master position x_m along the direction of impact for the tests described above using the position–position controller. Note that since there is no force sensor on the master device, the force felt by the human F_h is not directly available. Fortunately, since the Phantom is very light and easily back-drivable, the negative of the master control force, $-F_{cm}$, represents a good approximation to F_h.

The first thing to notice about the plots in Figure 14 is that stable contact is made in all four tests. Due to its inherent passivity, the position–position controller is very robust to changes in both environment and operator impedances, and the addition of model-based force control does not disrupt this robustness.

The lack of transparency of the position–position controller is also visible in these data sets. Once contact is made, the compliance in the system results in a loss of exact position tracking as the master must travel further than the slave in order to generate the contact force via the virtual spring. The inertia of the system also results in a lack of force tracking in free-space as the human must apply a force to accelerate the system to get it moving.

The addition of model-based force control around the slave significantly improves the transparency of the system by rejecting the internal friction forces in the slave. Most dramatic is the improvement in force tracking once steady state contact is made. For the tests without model-based control, the steady-state contact force is almost 50% less than the force felt by the human. The tests using the model-based control in contrast achieved perfect steady-state force tracking once the transients of impact died down.

The transparency improvements can also be seen in the free-space motion of the telerobot. With the model-based controller rejecting the friction in the slave, the force the human must apply to accelerate the telerobot is much smaller than when model-based control is not used. Similarly, once the robot has reached an approximately constant velocity before impact is made, the force applied by the human drops to zero when using model-based control as the human no longer needs to overcome friction to keep the robot moving.

5.2. 4-channel control

The 4-channel controller is designed to maximize transparency and gets its name from the fact it requires measurements of all four variables of interest; the operator force F_h, the environment force F_e, the master position x_m, and the slave position x_s. Developed independently by both Lawrence (1993) and Yokokohji and Yoshikawa (1994), the 4-channel controller consists of three elements: inverse dynamics of both master and slave to get exact position tracking, bilateral force feedback to obtain force tracking, and a bilateral position controller to help reject any disturbances or modeling errors.

Since implementing inverse dynamics requires both very accurate acceleration measurements and exact robot models, the inverse dynamics are typically not included in actual implementations. Furthermore, the lack of a force sensor on the master device used here further prohibits the implementation of a true 4-channel controller. Without an explicit measurement of F_h, the force felt by the operator must be approximated by F_{cm} resulting in the modified 4-channel controller shown in Figure 15. While these modifications will keep the 4-channel controller from achieving true transparency, the system should be transparent at steady state. For the results presented here, the position controller is the same PD controller used in the position–position controller with $K_p = 200$ N/m and $K_d = 6$ Ns/m.

5.2.1. Impact experiments. Figure 16 plots the forces and positions recorded when using the modified 4-channel telerobotic controller to contact both the stiff and soft environments. As expected, the modified 4-channel controller is not absolutely stable and as such it does not make stable contact with the aluminum block, but it can make stable contact with the much more forgiving foam.

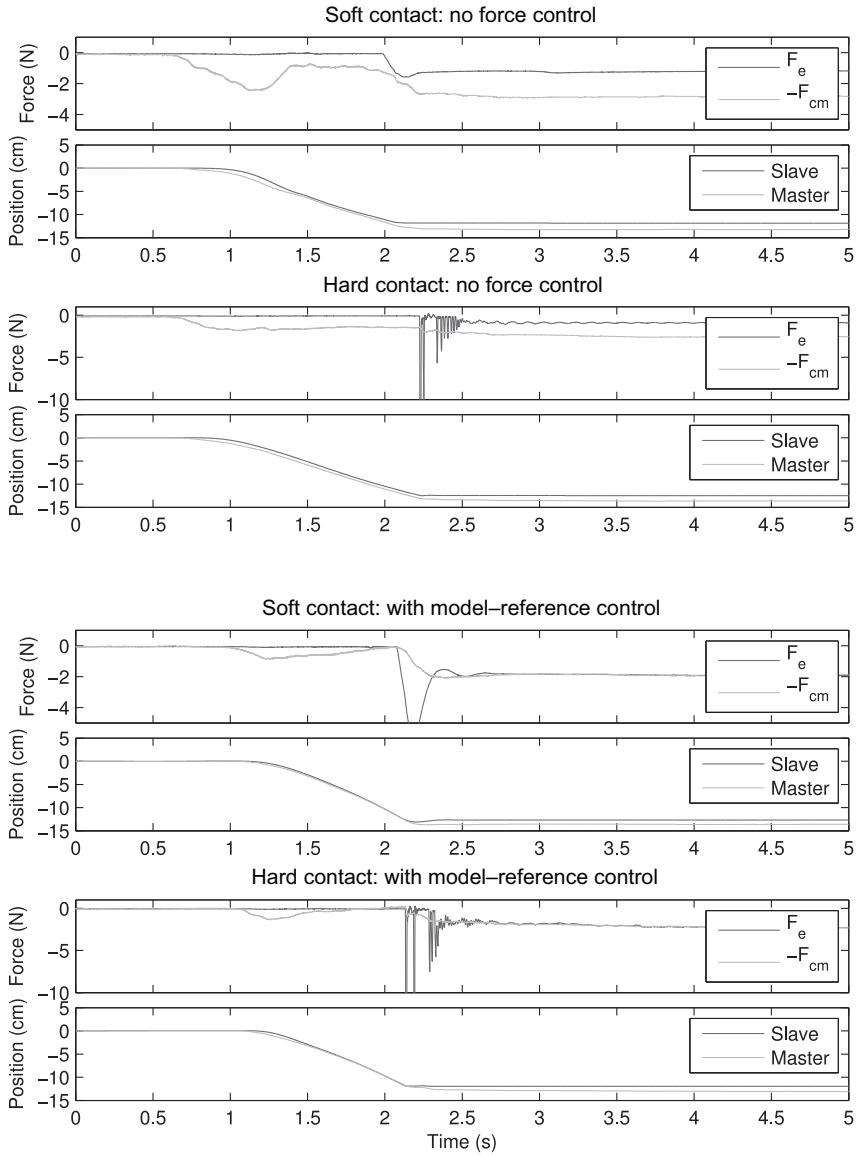

Fig. 14. Impact data for position–position-controlled telerobot with and without slave-side model-based control.

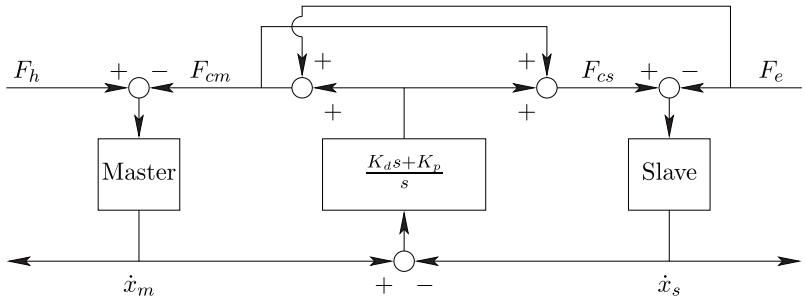

Fig. 15. Modified 4-channel telerobotic controller.

Without the use of model-based force control, the 4-channel controller does not achieve its promised transparency even at steady state. The friction in the slave is at least partially felt when moving at a constant velocity and the friction also keeps the environment force from tracking the applied human force when in contact. While it is hard to see from Figure 16 the friction in the slave also keeps the 4-channel controller from achieving true position tracking.

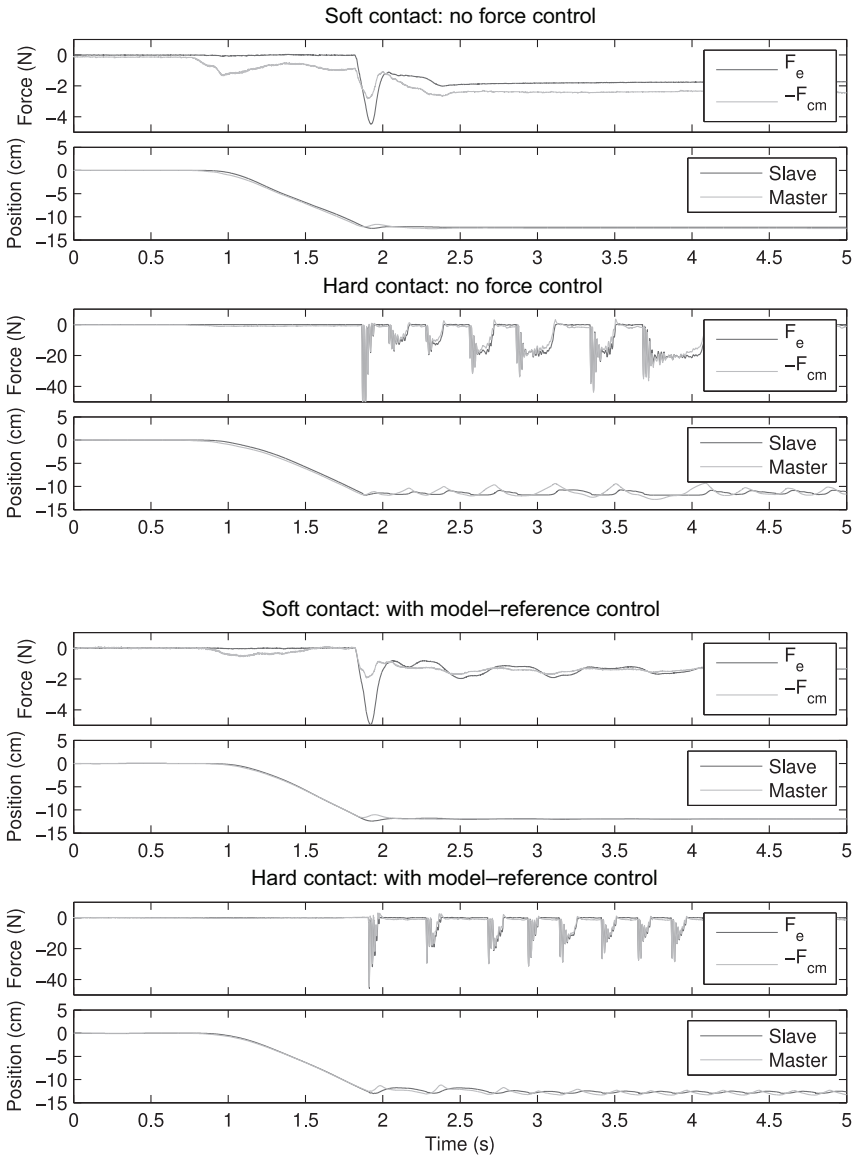

Fig. 16. Impact data for modified 4-channel telerobotic controller with and without slave-side model-based control.

The RMS position error for the last 2.5 s of the experiment when contacting the foam is 2.3 mm.

The addition of model-based force control on the other hand allows the 4-channel controller to achieve its true potential. By rejecting the friction in the system, the telerobotic system achieves steady state force tracking, and the RMS position error drops to 0.6 mm over the last 2.5 s of the test.

Its also worth looking at the unstable responses measured when the telerobot was attempting to make contact with the aluminum block. Each time the slave impacts the aluminum block, the force response is a combination of both a high-frequency oscillation at about 65 to 70 Hz and a lower frequency bouncing motion. It is interesting to note, the high-frequency oscillations are at about the same frequency both with and without model-based force control while the bouncing motion occurs more rapidly when using model-based control. The limited effect model-based control has upon the high-frequency oscillations suggests these oscillations are inherent to the 4-channel controller and most likely arise due to the bilateral force feedback terms. These high-frequency oscillations then excite the compliance in the position controller causing the telerobot to bounce away from contact. By rejecting the friction in the

slave, the model-based force controller effectively increases the resonant frequency of the position controller explaining why the slave bounces at a higher frequency.

6. Conclusion

As the demands on telerobotic systems grow more and more complex it is becoming crucial that telerobotic systems provide their human operators a detailed and accurate representation of the remote environment they are operating within. While the state of the art in telerobotic control architectures continues to advance the theoretical level of transparency that can be achieved, in actual implementations the resulting transparency is almost always less than predicted by the control designers. In most cases, the transparency is limited by the fundamental, and often non-ideal, dynamics of the master and slave robots.

The model-based force controller presented here can help improve transparency by rejecting the friction in the slave robot (and in the master too if applied around the master as well). Analytical results have shown model-based force control to be very robust when rejecting both Coulomb and viscous friction, while experimental results have shown robustness when subject to the efficiency reducing friction found in gearing.

In telerobotic systems that already utilize force measurements, there is very little risk and potentially a lot of reward to be had by introducing model-based force control. By not attempting to hide any of the robot's inertia, model-based force control results in closed-loop slave robots that are absolutely stable. As such, model-based control can be added to any standard telerobotic control architecture without worrying that it might decrease the overall robustness of the telerobot.

Funding

This work was supported by the National Aeronautics and Space Administration (NASA) via the Institute for Dexterous Space Robotics and through the National Science Foundation (NSF) through a graduate research fellowship.

References

Akin DL (2001) Science planning for the Ranger telerobotic shuttle experiment. In: *Proceedings of the 6th International symposium on artificial intelligence and robotics and automation in space*, Montreal, Canada, 18–22 June 2001.

Anderson RJ and Spong MW (1989) Bilateral control of teleoperators with time delay. *IEEE Transactions on Automatic Control* 34(5): 494–501.

Chiaverini S, Siciliano B and Villani L (1994) Force/position regulation of compliant robot manipulators. *IEEE Transactions on Automatic Control* 39(3): 647–652.

Colgate E and Hogan N (1989) An analysis of contact instability in terms of passive physical equivalents. In: *IEEE International conference on robotics and automation*, Scottsdale, AZ, 14–19 May 1989, pp. 404–409.

Daniel RW and McAree P (1998) Fundamental limits of performance for force reflecting teleoperators. *International Journal of Robotics Research* 17(8): 811–830.

Eppinger SD and Seering WP (1987) Understanding bandwidth limitations in robot force control. In: *IEEE International conference on robotics and automation*, Raleigh, NC, March 1987, Vol. 4, pp. 904–909.

Eppinger SD and Seering WP (1992) Three dynamic problems in robot force control. *IEEE Transactions on Robotics and Automation* 8(6): 751–758.

Franken M, Stramigioli S, Secchi C, et al. (2011) Bilateral telemanipulation with time delays: A two-layer approach combining passivity and transparency. *IEEE Transactions on Robotics and Automation* 27(4): 741–755.

Hannaford B (1989) A design framework for teleoperators with kinesthetic feedback. *IEEE Transactions on Robotics and Automation* 5(4): 426–434.

Hart JS (2010) *Absolutely stable force control for telerobotic applications*. PhD Thesis, Stanford University.

Hashtrudi-Zaad K and Salcudean SE (2002) Transparency in time-delayed systems and the effect of local force feedback for transparent teleoperation. *IEEE Journal of Robotics and Automation* 18(1): 108–114.

Hogan N (1985a) Impedance control: An approach to manipulation. Part I—Theory. *Journal of Dynamic Systems Measurement and Control—Transactions of the ASME* 107(1): 1–7.

Hogan N (1985b) Impedance control: An approach to manipulation. Part II—Implementation. *Journal of Dynamic Systems Measurement and Control—Transactions of the ASME* 107(1): 8–16.

Hogan N (1985c) Impedance control: An approach to manipulation. Part III—Applications. *Journal of Dynamic Systems Measurement and Control—Transactions of the ASME* 107(1): 17–24.

Hogan N (1988) On the stability of manipulators performing contact tasks. *IEEE Journal of Robotics and Automation* 4(6): 677–686.

Kazerooni H, Waibel BJ and Kim S (1990) On the stability of robot compliant motion control: Theory and experiments. *Journal of Dynamic Systems, Measurement, and Control—Transactions of the ASME* 112(3): 417–426.

Khatib O (1987) A unified approach for motion and force control of robot manipulators: The operational space formulation. *IEEE Journal of Robotics and Automation* 3(1): 43–53.

Kuchenbecker KJ and Niemeyer G (2006) Induced master motion in force-reflecting teleoperation. *Journal of Dynamic Systems, Measurement, and Control—Transactions of the ASME* 128: 800–810.

Lawrence DA (1993) Stability and transparency in bilateral teleoperation. *IEEE Transactions on Robotics and Automation* 9(5): 624–637.

Llewellyn FB (1952) Some fundamental properties of transmission systems. *Proceedings of the IRE* 40(3): 271–283.

Love LJ and Book WJ (2004) Force reflecting teleoperation with adaptive impedance control. *IEEE Transactions on Systems, Man, and Cybernetics—Part B: Cybernetics* 34(1): 159–165.

Mahvash M and Okamura A (2007) Friction compensation for enhancing transparency of a teleoperator with compliant transmission. *IEEE Transactions on Robotics* 23(6): 1240–1246.

Mahvash M and Okamura AM (2006) Friction compensation for a force-feedback telerobotic system. In: *IEEE International*

conference on robotics and automation, Orlando, FL, 15–19 May 2006, pp. 3268–3273.

Meys RP (1990) Review and discussion of stability criteria for linear 2-ports. *IEEE Transactions on Circuits and Systems* 37(11): 1450–1452.

Mills JK and Lokhorst DM (1993) Stability and control of robotic manipulators during contact/noncontact task transition. *IEEE Transactions on Robotics and Automation* 9(3): 335–345.

Newman WS (1992) Stability and performance limits of interaction controllers. *Journal of Dynamic Systems, Measurement, and Control—Transactions of the ASME* 114(4): 563–570.

Newman WS and Zhang Y (1994) Stable interaction control and Coulomb friction compensation using natural admittance control. *Journal of Robotic Systems* 11(1): 3–11.

Niemeyer G and Slotine JJE (2004) Telemanipulation with time delays. *The International Journal of Robotics Research* 23(9): 873–890.

Olsson H, Åström KJ, de Wit CC, et al. (1998) Friction models and friction compensation. *European Journal of Control* 4(3): 176–195.

Park J and Khatib O (2006) A haptic teleoperation approach based on contact force control. *International Journal of Robotics Research* 25(5-6): 575–591.

Raibert MH and Craig JJ (1981) Hybrid position/force control of manipulators. *Journal of Dynamic Systems, Measurement, and Control—Transactions of the ASME* 102(2): 126–133.

Richert D, Macnab CJB and Pieper JK (2012) Adaptive haptic control for telerobotics transitioning between free, soft, and hard environments. *IEEE Transactions on Systems, Man, and Cybernetics* 42(3): 558–570.

Rollett J (1962) Stability and power-gain invariants of linear twoports. *IRE Transaction on Circuit Theory* 9(1): 29–32.

Roy J and Whitcomb LL (2002) Adaptive force control of position/velocity controlled robots: Theory and experiment. *IEEE Transactions on Robotics and Automation* 18(2): 121–137.

Ryu JH, Kwon DS and Hannaford B (2004) Stable teleoperation with time-domain passivity control. *IEEE Transactions on Robotics and Automation* 20(2): 365–373.

Salisbury JK (1980) Active stiffness control of a manipulator in Cartesian coordinates. In: *IEEE conference on decision and control including the symposium on adaptive processes*, Albuquerque, NM, December 1980, Vol. 19, pp. 95–100.

Singh SK and Popa DO (1995) An analysis of some fundamental problems in adaptive control of force and impedance behavior: Theory and experiments. *IEEE Transactions on Robotics and Automation* 11(6): 912–921.

Slotine JJE and Li W (1991) *Applied Nonlinear Control*. Englewood Cliffs, NJ: Prentice Hall.

Tanner NA and Niemeyer G (2004) Improving perception in time-delayed telerobotics. *The International Journal of Robotics Research* 24(8): 631–644.

Wen JT and Murphy S (1991) Stability analysis of position and force control for robot arms. *IEEE Transactions on Automatic Control* 36(3): 365–370.

Wilfinger LS, Wen JT and Murphy SH (1994) Integral force control with robustness enhancement. *IEEE Control Systems Magazine* 14(1): 31–40.

Xu WL, Han JD, Tso SK, et al. (2000) Contact transition control via joint acceleration feedback. *IEEE Transactions on Industrial Electronics* 47(1): 150–158.

Yokokohji Y and Yoshikawa T (1994) Bilateral control of master–slave manipulators for ideal kinesthetic coupling—Formulation and experiment. *IEEE Transactions on Robotics and Automation* 10(5): 605–620.